Automatic Dynamic Estimation of On-Orbit Satellites Through Spaceborne ISAR Imaging

Yejian Zhou, Pengfei Xie, Chenwei Li, Mao Jian, Lei Zhang, and Wenan Zhang, *Member, IEEE*

***Abstract*— With the continuous development of satellite constellations worldwide, dynamic estimation of on-orbit spacecraft plays a more and more important role in space situation awareness applications. Based on high-resolution inverse synthetic aperture radar (ISAR) imaging from the ground, some exploratory methods have been proposed to estimate target dynamic parameters, such as its attitude pointing and spin period. Due to the limited observation view from the ground, most of them rely on the long-term measurement, and the robust association of image features needs to be ensured. In this article, a novel approach based on spaceborne ISAR images is proposed to achieve the dynamic estimation of spin satellites. In order to build a synchronous similar-resolution ISAR imaging system, two adjacent satellites are picked up from low earth orbit constellations according to the radar tracking parameters. With obtained a pair of ISAR images, the explicit expression between target dynamic parameters and projection feature is deduced. Inspired by the existing works on shape extraction of the human body, a feature extraction network is built on the framework of ResNet for achieving the automatic processing in spaceborne equipments. In this way, target dynamic parameters can be solved in instantaneous attitude optimization and spin motion optimization in steps. Simulation experiments of a typical spin spacecraft, Tiangong-I, illustrate the feasibility of the proposed method. Besides, a comparison experiment with an existing ground-based work is also made to analyze its advantage in practical applications.**

***Index Terms*— Dynamic estimation of satellites, ISAR imaging, bi-station spaceborne radar, automatic shape extraction.**

I. Introduction

DYNAMIC estimation of on-orbit satellites has attracted tremendous attention in the space situation awareness (SSA) field [1], [2]. As mega-constellations (like SpaceX's Starlink Program) are continuously built over the world, the current space orbit resource is further compressed and the risk of collision among low earth orbit (LEO) satellites increases [3], [4], [5]. The satellite collision will generate a large amount of debris, threatening the security of nearby satellites. In order to analyze the collision probability between satellites, the real-time dynamic information of on-orbit Satellites is expected. However, when satellites lose connection with the ground, it is hard to estimate their dynamic parameters through most ego-motion estimation methods relying on either the inertial navigation system or the observation data conveyed from the target [6], [7]. In this case, it proves essential to obtain the dynamic parameters of on-orbit satellites from external observation for the collision probability analysis [8], [9], [10], [11], [12].

Reviewing the relevant works on satellite monitoring, we know that inverse synthetic aperture radar (ISAR) has been widely used to estimate the state parameters of on-orbit satellites because of its high-resolution and all-weather detection capability [13], [14], [15], [16], [17], [18], [19], [20], [21], [22], [23], [24], [25], [26]. For example, Tracking and Imaging Radar (TIRA) was applied to track Envisat from 2011 to 2017. Even though Envisat has lost connection with the ground station, its spin period and other dynamic parameters can still be estimated through a corresponding imaging simulation software [13], [14], [15]. Similarly, the target RCS sequence measured by the ground-based ISAR is also used to match the simulation data, and the target state parameters can be determined by similarity optimization [16]. Besides, inspired by the existing structure from motion (SFM) works in the computer vision field, some researchers propose to extract the observation matrix of the target scattering points from multi-look ISAR images, and then decompose it to recover three-dimensional (3D) structure of the satellite by the Singular Value Decompose (SVD) algorithm [17], [18], [19]. Moreover, using mathematical expression between the target state and its ISAR image features to obtain target dynamic parameters is another potential approach [20], [21]. For example, multiple station ISAR images are used to determine the attitude and spin period of spin satellites [20]. However, since most existing methods are based on the ground equipment, their performances are limited by the ground observation view and the low frequency band [22], [23], [24], [25], [26]. As a result, it is hard to use these methods for the state monitoring of the constellation. On the other hand, with various sensors mounted on constellations, we can adopt spaceborne high-resolution ISAR imaging to achieve the dynamic estimation of on-orbit satellites [27], [28], [29], [30]. Compared with ground-based equipments, space-borne ISAR equipments can obtain more

Manuscript received 10 November 2022; revised 21 January 2023 and 24 March 2023; accepted 12 April 2023. Date of publication 17 April 2023; date of current version 25 April 2023. This work was supported in part by the National Natural Sciences Foundation of China under Grant 62101494, in part by the Zhejiang Provincial Natural Science Foundation of China under Grant LY23F010012, and in part by the Shenzhen Science and Technology Program under Grant KQTD20190929172704911. *(Corresponding authors: Pengfei Xie; Yejian Zhou.)*

Yejian Zhou, Chenwei Li, and Wenan Zhang are with the College of Information Engineering, Zhejiang University of Technology, Hangzhou 310023, China (e-mail: yjzhou25@zjut.edu.cn).

Pengfei Xie and Lei Zhang are with the School of Electronics and Communication Engineering, Sun Yat-sen University (Shenzhen Campus), Shenzhen 518100, China (e-mail: PerfeiShieh@126.com).

Mao Jian is with the Laboratory of Pinghu, Beijing Institute of Infinite Electric Measurement, Pinghu, 314200, China.

Digital Object Identifier 10.1109/TRS.2023.3267739

observation angle resource for a certain target by using the adjacent observation satellites or changing the orbits of several satellites in a constellation. The multi-look observation feasibility benefits the information acquisition of the on-orbit satellite. And the observation strategy of spaceborne radars is more flexible than that of existing ground-based methods.

Hence, a novel on-orbit satellite dynamic estimation method based on synchronous bi-station spaceborne ISAR imaging is proposed in this paper. A mathematical expression is derived to describe the intrinsic relation between the target dynamic parameters and acquired range-Doppler (RD) images. The angular diversity of bi-station images is employed to separate the target instantaneous attitude estimation from the imaging geometry determination when the target spins. After that, the estimated target attitude parameters are used to solve target spin parameters. A brief flow of the proposed method is given below. At first, two adjacent satellites are selected according to the radar LOS sequence for synchronous imaging, and a bi-station spaceborne observation system is built for a certain target satellite. After the synchronous imaging processing, target structure features are extracted automatically from the ISAR images by using a feature extraction network based on the framework of ResNet [31], [32], [33]. Finally, the acquired target projection lengths are substituted into the target attitude and spin optimizations, which are solved by the chaotic grasshopper optimization algorithm (CGOA) [34], [35].

Compared with the existing works, the contributions of the proposed algorithm are as follows.

1) To the best of our knowledge, it is the first time that the spaceborne ISAR system has been used for the dynamic parameter estimation of on-orbit satellites based on the bi-station spaceborne observation. Since the bi-station spaceborne observation breaks up the imaging view limitation of the ground-based observation, the proposed algorithm not only becomes robust in solving target dynamic optimization, but also can achieve continuous monitoring for a certain target with an LEO constellation. From the view of SSA applications, it has a potential capacity for the security maintenance of meta-constellations.
2) An automatic feature extraction framework is designed to describe target structures. According to the feature extraction framework, the target scattering points can be precisely extracted so as to determine target projection features in ISAR images. This automatic feature extraction framework is the core to perform all steps of the proposed method in the spaceborne device, including high-resolution imaging, feature extraction, and target dynamic estimation. It is beneficial to develop the practical application value of the meta-constellation.

The remainder of the paper is organized as follows. In Section II, the fundamental of the proposed algorithm is introduced, and the synchronous imaging geometry of the bi-station spaceborne ISAR observation is developed. The motion model of the on-orbit satellite is utilized to derive an explicit expression to associate target dynamic parameters with image features. The proposed method is presented in Section III. It consists of three key steps, i.e. bi-station system

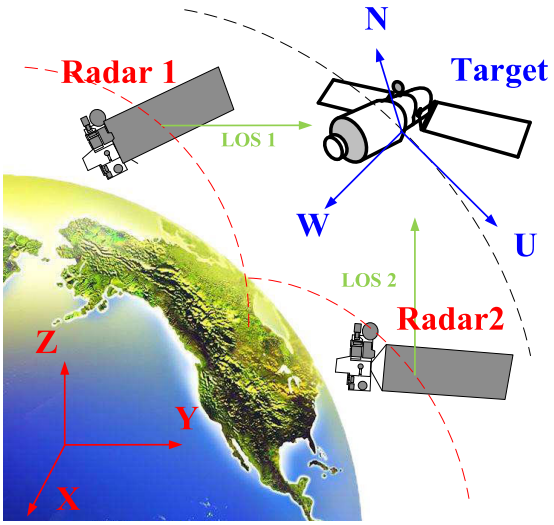

Fig. 1. The spaceborne observation model in the ECEF coordinate system.

building, image feature extraction, and target dynamic estimation, which are described in detail. Section IV demonstrates the feasibility and advantages of the proposed algorithm through three simulation experiments. Some crucial conclusions are drawn in Section V.

II. The Fundamentals of Target Dynamic Estimation

In this section, the fundamental of the proposed method is introduced. The geometric model of the spaceborne ISAR imaging and the motion model of spin targets are analyzed, respectively. Based on these two models, an explicit expression is developed to establish the relationship between the target image feature and the target dynamic parameters.

A. The ISAR Imaging Model of Spaceborne Observation

In order to describe the ISAR imaging geometry of target orbit motion and spin motion, we establish two sets of coordinate systems, as shown in Fig.1. One is the Earth-Centered Earth-Fixed (ECEF) coordinate system, which is used to describe the relative motion between the target and spaceborne radars. The other is the target Cartesian coordinate system, which is used to describe the target attitude and spin parameters. In the target Cartesian coordinate system, the N axis always points to the earth's core, and U axis is tangent to the target orbit and keeps up with the target trajectory motion. According to the right-hand rule, N axis and U axis determine W axis, which is along the normal direction of the trajectory plane.

As shown in Fig.1, the positions of both target and spaceborne radars can be determined with their Two Line Element (TLE) parameters in the ECEF coordinate system. The instantaneous radar line of sight (LOS) vector is below:

$$\vec{\mathbf{k}}(x,y,z)=\frac{\vec{\mathbf{q}}_{tg}(x,y,z)-\vec{\mathbf{q}}_{ob}(x,y,z)}{\left|\vec{\mathbf{q}}_{tg}(x,y,z)-\vec{\mathbf{q}}_{ob}(x,y,z)\right|} \tag{1}$$

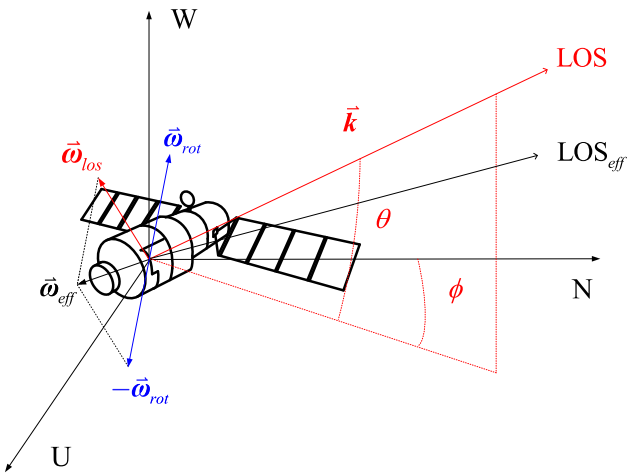

Fig. 2. The ISAR imaging observation model in the target Cartesian coordinate system.

where $\vec{\mathbf{q}}_{ob}(x, y, z)$ represents the 3D coordinates of the observation satellite, and $\vec{\mathbf{q}}_{tg}(x, y, z)$ represents the 3D coordinates of the target satellite.

In order to match the turntable model in the classical ISAR imaging algorithm, the instantaneous radar LOS vector is converted to the below equation under the target Cartesian coordinates, as shown in Fig. 2.

$$\vec{\mathbf{k}}(n, u, w) = \mathbf{R}(t_m) \bullet \vec{\mathbf{k}}(x, y, z) \tag{2}$$

where $\mathbf{R}(t_m)$ is the transformation matrix between the ECEF coordinate system and target Cartesian coordinate system, which can be calculated according to the real-time positions of the target satellite and spaceborne satellites.

The ISAR imaging contribution of trajectory is described with the time-variant LOS vector $\vec{\mathbf{k}}(n, u, w)$. It is centered at the target centroid and oriented toward the observation radar. As a unit vector, the instantaneous radar sight direction $\vec{\mathbf{k}}$ also can be represented with two angle parameters, elevation angle θ_{los} and azimuth angle ϕ_{los}, as follows.

$$\begin{aligned}\vec{\mathbf{k}}(\theta_{\text{los}}, \phi_{\text{los}}) = (&\cos\theta_{\text{los}}(t_m)\sin\phi_{\text{los}}(t_m),\\ &\cos\theta_{\text{los}}(t_m)\cos\phi_{\text{los}}(t_m), \sin\theta_{\text{los}}(t_m))^{\text{T}}\end{aligned} \tag{3}$$

where t_m denotes the slow-time relative to the azimuth sampling, elevation angle $\theta_{\text{los}}(t_m)$ is the intersection angle between instantaneous radar LOS vector and the NOU plane, and the azimuth angle $\phi_{\text{los}}(t_m)$ is the intersection angle between U axis and the projection of instantaneous radar LOS vector on the NOU plane.

Then, the rotation of spin satellite is also expressed through two angle parameters. For the observation of LEO satellites, the single imaging period is about several seconds, while the spin period of satellite is around hundreds of seconds in most cases [36]. Therefore, the satellite spinning can be regarded as the satellites rotation around a certain shaft at a constant speed during the single imaging period. Different target spin patterns can be expressed by the change of rotation shaft and speed parameters in long-term observation. The spin motion is defined by the following equation.

$$\vec{\mathbf{w}}_{\text{rot}} = (\cos\theta_{\text{rot}}\sin\phi_{\text{rot}}, \cos\theta_{\text{rot}}\cos\phi_{\text{rot}}, \sin\theta_{\text{rot}})^{\text{T}}\omega_{rot} \tag{4}$$

where ω_{rot} is the rotation speed, the elevation angle θ_{rot} is the intersection angle between the rotation shaft vector and the NOU plane, and the azimuth angle ϕ_{rot} is the intersection angle between U axis and the projection of the rotation shaft vector on the NOU plane.

After the motion compensation in the range-Doppler algorithm, the azimuth scaling of the ISAR image depends on the effective rotation $\vec{\mathbf{w}}_{\text{eff}}$ between the target scattering points and radar. When the target spins, both the rotation of LOS angle $\vec{\mathbf{w}}_{\text{los}}$ and the target spin motion $\vec{\mathbf{w}}_{\text{rot}}$ ought to be taken into consideration of effective rotation determination.

$$\vec{\mathbf{w}}_{\text{eff}} = \vec{\mathbf{w}}_{\text{los}} - \vec{\mathbf{w}}_{\text{rot}} \tag{5}$$

During the single imaging period, $\vec{\mathbf{w}}_{los}$ can be calculated according to the LOS vectors at start and end moments. However, the target spin parameters are unknown in this work. Therefore, the azimuth scaling can not be performed after azimuth compensation.

B. The Target Dynamic Estimation From Spaceborne ISAR Images

From the analysis of spaceborne ISAR observation in the former section, we know that associating the spin motion with the observed ISAR image features becomes the key point in the dynamic estimation of spin satellites. According to the ISAR imaging projection theory proposed in [37], ISAR imaging can be equivalent to the geometric projection of the target on the radar imaging plane. If the ISAR image are scaled in the two dimensions, the target dynamic parameters, including attitude vectors and motion period, can be directly estimated with the projection equations. Therefore, we propose a bi-station joint imaging strategy to estimate the target instantaneous attitude at first. Then, by using the solved instantaneous attitude vectors, target Doppler information is extracted from ISAR images to build another spin parameter optimization. Detailed derivations are presented below.

As shown in Fig. 3, the unit vectors of the range axes in the bi-station ISAR images are given in the target Cartesian coordinate system. When the central moments of ISAR imaging are synchronous and considered as the reference time, the spin motion does not affect the calculation of the instantaneous equivalent radar LOS. As a result, the projection lengths of two typical structures along the range axis, the spacecraft body and the solar wing, are expressed as

$$R_{i,j} = \vec{\mathbf{k}}_i \bullet \vec{\mathbf{l}}_j L_j \tag{6}$$

$$\vec{\mathbf{l}}_j = \left(\cos\alpha_j \sin\beta_j, \cos\alpha_j \cos\beta_j, \sin\alpha_j\right)^{\text{T}} \tag{7}$$

where $\vec{\mathbf{l}}_j$ is the attitude vector of the j-th structure, α is the intersection angle between the attitude vector and the NOU plane, β is the intersection angle between U axis and the projection of the attitude vector on the NOU plane, L refers to the prior length, $\bullet$ denotes the inner product, and the subscript of $\vec{\mathbf{k}}_i$ represents the series of the spaceborne radars.

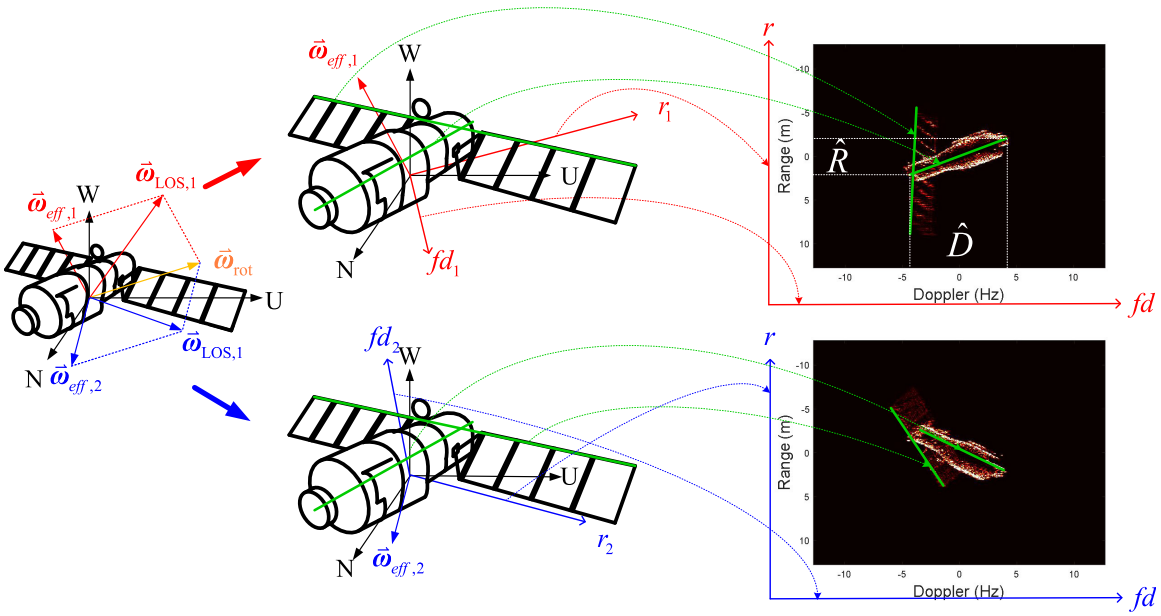

Fig. 3. The target ISAR image interpretation by the ISAR imaging projection theory.

Besides, the orthogonality relationship of these two structures is considered in this paper. Thus, the joint attitude optimization of two typical structures is built as follows.

$$\begin{aligned} &\underset{\alpha_1,\alpha_2,\beta_1,\beta_2}{\arg\min} \quad \sum_{j=1}^{2}\left(\vec{\mathbf{k}}_1 \bullet \vec{\mathbf{l}}_j L_j - \hat{R}_{1,j}\right)^2 + \left(\vec{\mathbf{k}}_2 \bullet \vec{\mathbf{l}}_j L_j - \hat{R}_{2,j}\right)^2 \\ &s.t. \quad \tan\alpha_1 \tan\alpha_2 + \cos(\beta_1 - \beta_2) = 0 \end{aligned} \tag{8}$$

where $\hat{R}_{i,j}$ represents the extracted range length of the j-th typical structure in the i-th imagery.

With the obtained parameters $\left(\tilde{\alpha}_1, \tilde{\beta}_1, \tilde{\alpha}_2, \tilde{\beta}_2\right)^T$, the attitude vectors of these two typical structures can be determined according to Eq. (7).

$$\tilde{\vec{\mathbf{l}}}_1 = \left(\cos\tilde{\alpha}_1 \sin\tilde{\beta}_1, \cos\tilde{\alpha}_1 \cos\tilde{\beta}_1, \sin\tilde{\alpha}_1\right)^{\mathrm{T}} \tag{9}$$

$$\tilde{\vec{\mathbf{l}}}_2 = \left(\cos\tilde{\alpha}_2 \sin\tilde{\beta}_2, \cos\tilde{\alpha}_2 \cos\tilde{\beta}_2, \sin\tilde{\alpha}_2\right)^{\mathrm{T}} \tag{10}$$

After that, both target instantaneous attitude and target trajectory are known, and can be directly used to estimation target spin parameters. At first, we can combine Eq.(5) and the below equation to calculate each image's imaging Doppler direction vector.

$$\vec{\mathbf{fd}}_i = \frac{\vec{\mathbf{k}}_i \times \vec{\mathbf{w}}_{eff,i}\left(\vec{\mathbf{w}}_{\mathrm{LOS},i}, \vec{\mathbf{w}}_{\mathrm{rot}}\right)}{\left\|\vec{\mathbf{k}}_i \times \vec{\mathbf{w}}_{eff,i}\left(\vec{\mathbf{w}}_{\mathrm{LOS},i}, \vec{\mathbf{w}}_{\mathrm{rot}}\right)\right\|} \tag{11}$$

where $\times$ is the cross product, $\|*\|$ indicates to the modulus of the vector, and the subscript of $\vec{\mathbf{k}}_i$ refers to the series of the spaceborne radars.

According to Eq. (6), the projection length of the typical structure on the Doppler direction is expressed as

$$d_{i,j} = \vec{\mathbf{fd}}_i \bullet \vec{\mathbf{l}}_j L_j \tag{12}$$

Then, the target spin state optimization is expressed as

$$\underset{\theta_{\mathrm{rot}},\phi_{\mathrm{rot}},\omega_{rot}}{\arg\min} \sum_{j=1}^{2}\left(\vec{\mathbf{fd}}_1 \bullet \vec{\mathbf{l}}_j L_j - \hat{D}_{1,j}\right)^2 + \left(\vec{\mathbf{fd}}_2 \bullet \vec{\mathbf{l}}_j L_j - \hat{D}_{2,j}\right)^2 \tag{13}$$

where $\hat{D}_{1,j}$ and $\hat{D}_{2,j}$ represent the Doppler size extraction of typical structures in these bi-station images, respectively, j refers to the number of typical structures.

III. The Target Dynamic Estimation Based on the Spaceborne ISAR Synchronous Imaging

The proposed algorithm for satellite dynamic estimation is comprised of two stages: the linkage stage and the interpretation stage. In the first stage, a bi-station spaceborne observation system is built according to the radar LOS sequences for synchronous imaging. After that, the projection feature of the ISAR image is extracted to estimate target dynamic parameters in two optimizations, i.e. attitude optimization and spin optimization. The flowchart of the proposed method is depicted in Fig.4, and the detailed steps are as follows.

- Step 1. According to the target position in the ECEF system, several adjacent satellites are chosen as the potential agents of the spaceborne observation system.
- Step 2. Based on the TLE parameters, the radar LOS sequence of each satellite is calculated to determine the observation geometry. Then, the bi-station synchronous ISAR imaging system is built to obtain two ISAR images with the same resolution.
- Step 3. Once the synchronous images are generated, the key points of the target structures are extracted by the proposed feature extraction network. Based on these points, target projection feature of each typical structure is determined.

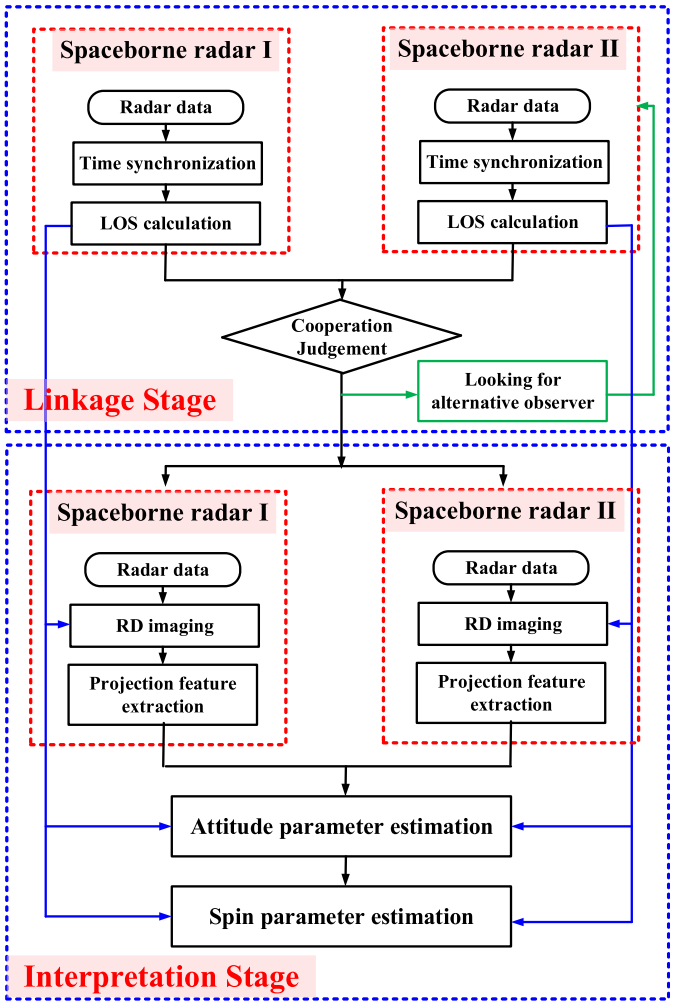

Fig. 4. The flowchart of the proposed algorithm.

- Step 4. The LOS parameters of the bi-station system and the extracted projection information on the range dimension of each ISAR image are substituted into Eq. (8) to estimate the target instantaneous attitude parameters.
- Step 5. Based on the estimation result of the target attitude, the extracted projection information on the Doppler dimension of each ISAR image is substituted into Eq. (13) to estimate the target spin parameters.

The key steps of the proposed approach are discussed as follows.

A. The Linkage of Bi-Station Spaceborne ISAR Imaging

According to the observation premise of the proposed method, the synchronous ISAR imaging of two adjacent satellites is established. Similar to the link visibility analysis of the LEO satellite constellation [38], [39], both the observation distance and antenna steering of the radar measuring ought to be taken into consideration of the tracking visibility. The central antenna angle is defined as the line of sight between the target and observation satellite, as shown in Fig. 5. It can be simulated with their TLE parameters in Satellite Tool Kit (STK) software. In practical applications, the LOS parameter also can be loaded from the tracking system on the satellites.

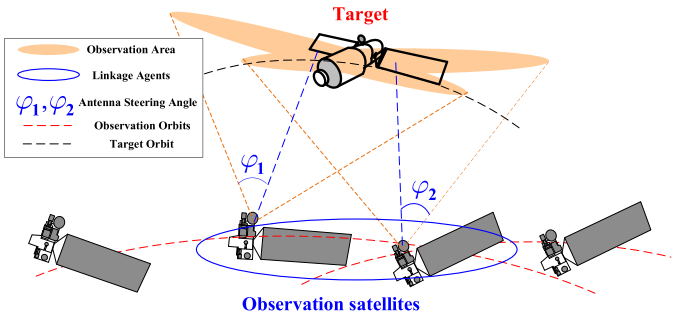

Fig. 5. The linkage of bi-station spaceborne sensors.

Then, the central LOS vector is transformed under the target Cartesian coordinates according to Eqs. (1)-(2). In this way, the service availability of bi-station synchronous ISAR imaging can be judged according to imaging resolution calculation. Usually, a 0.01-second synchronization accuracy is required for this task, which can be guaranteed by using the GPS system mounted on the satellite.

Unlike the optical imaging, the imaging resolutions of two dimensions in ISAR images are obtained in different ways. The range resolution of the image is related to the sampling frequency in the quick-time domain. In fact, it depends on the bandwidth of the radar signal, and the sampling frequency is determined under the Nyquist Sampling theorem.

$$\rho_r = c/2f_s \tag{14}$$

where f_s denotes the radar sampling frequency, and c represents the speed of light.

The image Doppler resolution depends on the coherence accumulation in the slow-time domain.

$$\rho_{fd} = \lambda/2\Delta\mathrm{T} \tag{15}$$

where ΔT refers to the time accumulation of single frame image, and λ is the signal wavelength.

As the effective rotation $\vec{\mathbf{w}}_{\mathrm{eff}}$ equals the rotation of the LOS angle $\vec{\mathbf{w}}_{\mathrm{los}}$ for the attitude-stabilized target, $\vec{\mathbf{w}}_{\mathrm{los}}$ can be transformed into the azimuth calibration according to the below equations.

$$\rho_a = \lambda/2\Delta\theta \tag{16}$$

$$\begin{aligned}\Delta\theta &= \vec{\mathbf{w}}_{\mathrm{eff}}\Delta\mathrm{T} \\ &= \vec{\mathbf{w}}_{\mathrm{LOS}}\Delta\mathrm{T}\end{aligned} \tag{17}$$

From the previous experience on the measured ISAR image [36], though the azimuth calibration can not be achieved when the target spins, the rotation of the LOS angle is still used to estimate the azimuth resolution. After that, two satellites that have similar imaging resolutions are chosen among previous potential agents, and the bi-station spaceborne ISAR imaging is established.

B. Projection Feature Extraction by Key Point Extraction Network

As the number of observation images rapidly increases in the satellite monitoring tasks, automatic feature extraction

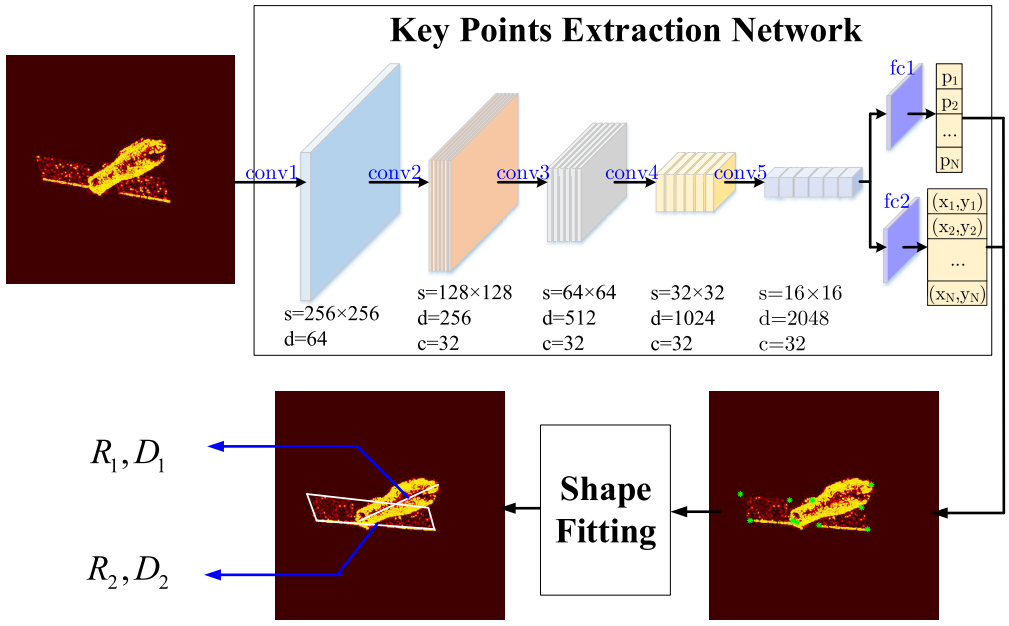

Fig. 6. The framework of the proposed feature extraction method.

plays a more and more important role. It directly affects the precision of solving target dynamic optimization. Inspired by the existing works on shape extraction of the human body [40], [41], [42], [43], we design a refined key point extraction network to extract target key points. Then, the 2D projection lengths of the target typical structure are obtained after shape fitting.

Take TG-I for an example. The vertices of solar wings and the endpoints of the target symmetry axis on its body are picked up as the key points. As shown in Fig.6, a three-layer Resnet is adopted as the backbone network, and an additional convolutional layer is used after the feature mapping. In this way, the serial number of points and their coordinates are obtained as the output. The loss function of the key point extraction network according to residual learning as below,

$$Loss = \sum_{i=1}^{10} |e_i - \hat{e}_i| + |o_i - \hat{o}_i| + \left\| \vec{\mathbf{p}}_i - \hat{\vec{\mathbf{p}}}_i \right\| \qquad (18)$$

where e_i is the classification loss of the existing confidence for the i-th point, e_i denotes the classification loss of the intermediate supervision for the i-th point, and $\vec{\mathbf{p}}_i$ represents the position loss of the i-th points in the RD image.

As for the details of network training, the definition of key points is different between different targets. In this paper, we define 10 key structural points as the key points of the TG-I. During training processing, the gradient descent method is used to make the predicted value close to the ground-truth. Once the coordinates of these ten points are obtained, the projection feature of the target body (R_1, D_1) can be determined with the first two points. Then, the remaining points are used to generate a parallelogram with polygon fitting. The projection feature of the long side (R_2, D_2) is obtained to describe the solar wing.

TABLE I
THE MAIN PARAMETERS OF THE ISAR IMAGE DATASET

Size of a single image	512×512
Center frequency of the transmit signal	10 GHz
Bandwidth	1 GHz
Pulse repetition frequency	100 Hz
Number of the observation angle	800

C. The Optimization Technique of the Target Dynamic Estimation

With the target projection feature extracted from the bi-station ISAR images, target dynamic parameters are estimated in two optimizations, one is the attitude parameter optimization in Eq.(8) and the other is the spin parameter optimization in Eq.(13). In order to solve these optimizations, the chaotic grasshopper optimization algorithm (CGOA) is adopted [34], [35]. Like most heuristic optimization methods, this method is divided into the exploration and exploitation stages for searching the best particle in the swarm. In the exploration stage, each particle in the swarm moves toward the food. During the exploitation period, the movement of the particle depends on its position in the swarm, which is also called the swarm interaction. The details are given in **Algorithm 1**.

Apart from other intelligent methods, the chaotic theory is employed to accelerate its global convergence speed and prevent it from trapping into a local optimum [35]. In this work, the circle map is adopted.

$$c(t+1) = \left(c(t) + b - \frac{P}{2\pi} \sin(2\pi c(t)) \right) \bmod (1) \qquad (19)$$

where the control parameters P and b are set to 0.5 and 0.2, respectively.

In the first optimization, as shown in Eq. (8), the unknown target attitude parameters $(\alpha_1, \beta_1, \alpha_2, \beta_2)$ are used to describe

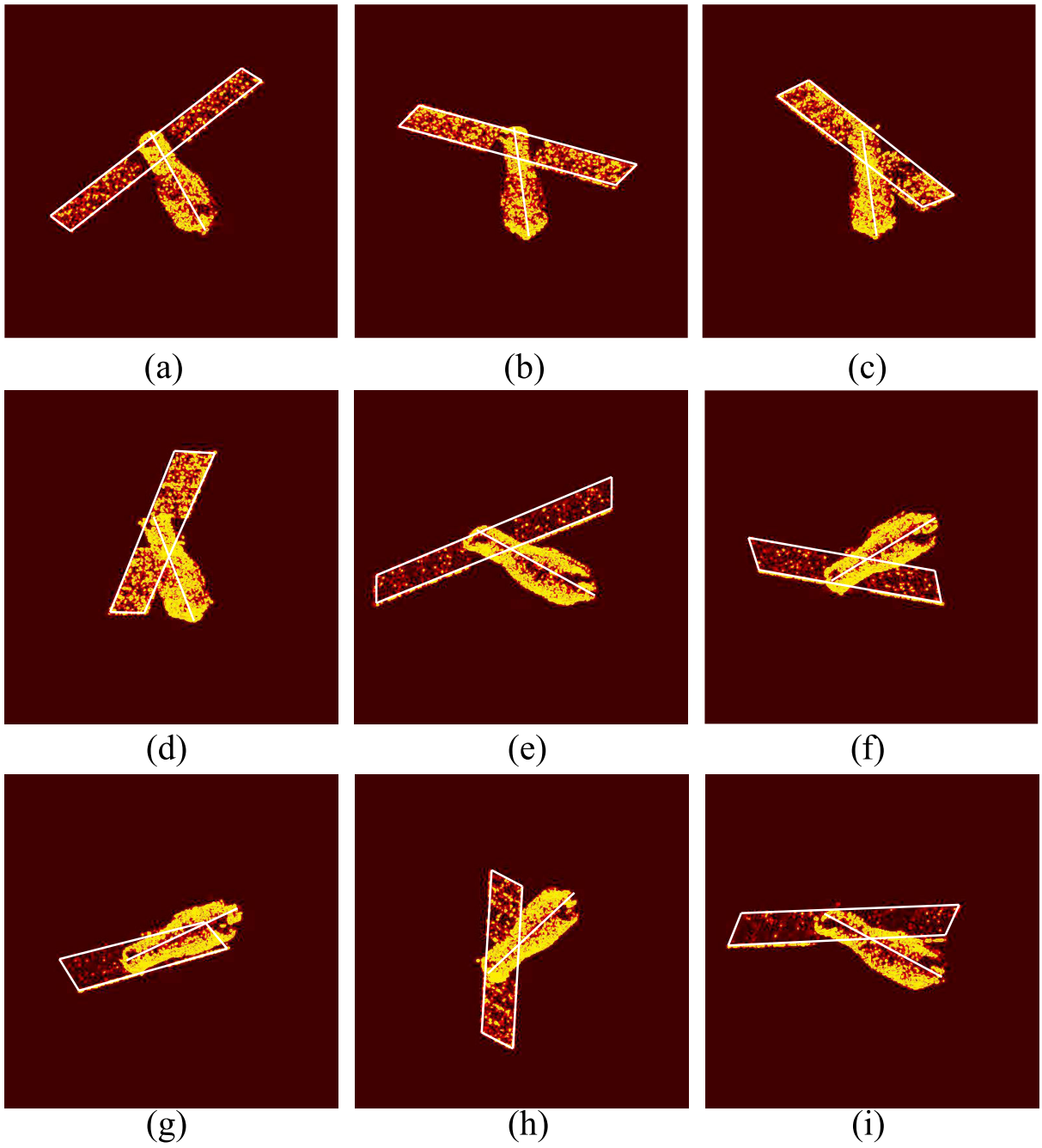

Fig. 7. The vision result of automatic feature extraction in RD images.

the particle position in CGOA.

$$\vec{X}_i = (\alpha_1, \beta_1, \alpha_2, \beta_2)^T \tag{20}$$

The fitness function is defined under the prior orthogonality restriction of target structures as follows.

$$J = \sum_{j=1}^{2} \left(\vec{\mathbf{k}}_1 \bullet \vec{\mathbf{l}}_j L_j - \hat{R}_{1,j}\right)^2 + \left(\vec{\mathbf{k}}_2 \bullet \vec{\mathbf{l}}_j L_j - \hat{R}_{2,j}\right)^2 + a_1 |\tan\alpha_1 \tan\alpha_2 + \cos(\beta_1 - \beta_2)| \tag{21}$$

where the confidence factor a_1 ensures the orthogonality restriction, and set to be 0.95 in this paper.

Similarly, the solution of spin parameter optimization Eq. (13) is defined as follows.

$$\vec{X}_i = \left(\theta_{\text{rot}}, \phi_{\text{rot}}, \omega_{rot}\right)^T \tag{22}$$

And its fitness function is drawn as follows.

$$J = \sum_{j=1}^{2} \left(\vec{\mathbf{fd}}_1 \bullet \vec{\mathbf{l}}_j L_j - \widehat{D}_{1,j}\right)^2 + \left(\vec{\mathbf{fd}}_2 \bullet \vec{\mathbf{l}}_j L_j - \widehat{D}_{2,j}\right)^2 \tag{23}$$

TABLE II
THE PERFORMANCE COMPARISON BETWEEN THE PROPOSED ALGORITHM AND GROUND TRUTH

-	Automatic extraction (pixels)		Ground truth (pixels)		-
Image Number	(R_1, D_1)	(R_2, D_2)	(R_1, D_1)	(R_2, D_2)	Mean bias (pixels)
1	(293.7, 228.8)	(-84.3,149.7)	(291.2,231.9)	(-82.7,143.0)	3.5
2	(-333.9,-90.4)	(-22.7,-166.8)	(-336.9,-86.2)	(-19.1,-173.2)	4.3
3	(-223.2,-173.4)	(-22.4,-161.3)	(-219.5,-176.6)	(-28.3,-167.5)	4.8
4	(103.6,-246.3)	(-61.8,-159.3)	(96.2,-243.4)	(-67.4,-154.8)	5.1
5	(-361.5,148.4)	(-181.7,-100.4)	(-368.3,149.3)	(-180.9,-93.75)	3.8
6	(-283.4,-50.4)	(-160.1,96.8)	(-280.9,-51.9)	(-160.3,99.5)	1.7
7	(-225.7,60.7)	(-170.5,79.9)	(-224.1,54.1)	(-164.6,74.4)	4.9
8	(-14.8,249.3)	(-132.9,123.9)	(-14.4,253.5)	(-128.4,127.2)	3.1
9	(-334.4,14.5)	(-180.9,-97.2)	(-330.9,12.1)	(-177.4,-103.0)	3.8

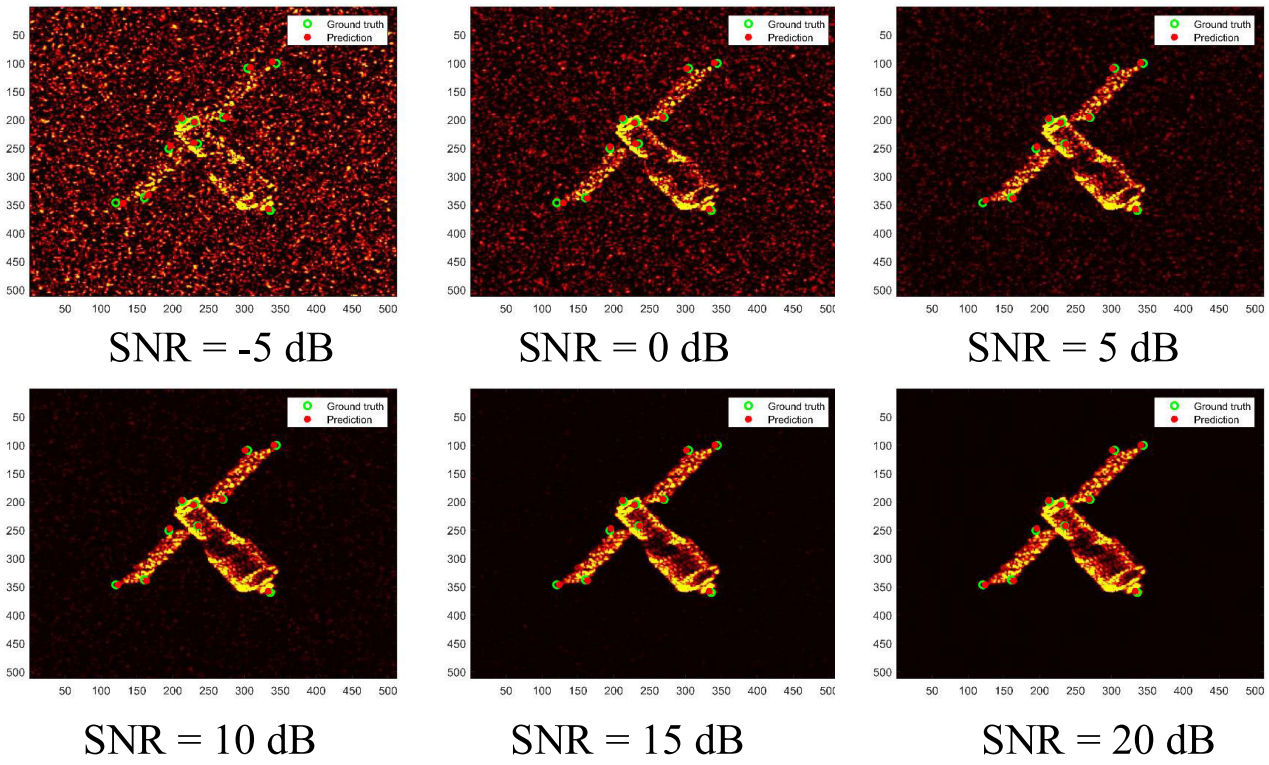

Fig. 8. Extraction results of TG-I in different noise conditions.

TABLE III
THE TLE PARAMETERS OF OBSERVERS AND TARGET SATELLITE IN THE OBSERVATION SCENE

Satellites	TLE parameters
Observer satellite 1	1 47787U 21018A 21357.37660384 .00000008 00000-0 19416-4 0 9993 2 47787 53.0546 312.8953 0001740 49.7388 310.3753 15.06395168 44543
Observer satellite 2	1 47789U 21018C 21357.23838029 .00000341 00000-0 41801-4 0 9996 2 47789 53.0557 293.5117 0001955 37.6591 322.4534 15.06397453 45152
Target satellite	1 03673U 69010B 22059.95073802 .00000069 00000-0 34660-3 0 9994 2 03673 80.3959 26.7087 0023248 192.4956 221.8937 12.63439798445276

IV. EXPERIMENT ANALYSIS

In this part, three experiments are designed to confirm the feasibility of the proposed algorithm. As the real ISAR data of on-orbit satellites is not public, these experiments will be performed on simulation data. The details are as follows.

- First, the proposed image feature extraction method is tested in a simulated dataset. The ground truth can be calculated directly because the imaging view, target 3D model, and instantaneous attitude of each image are known.

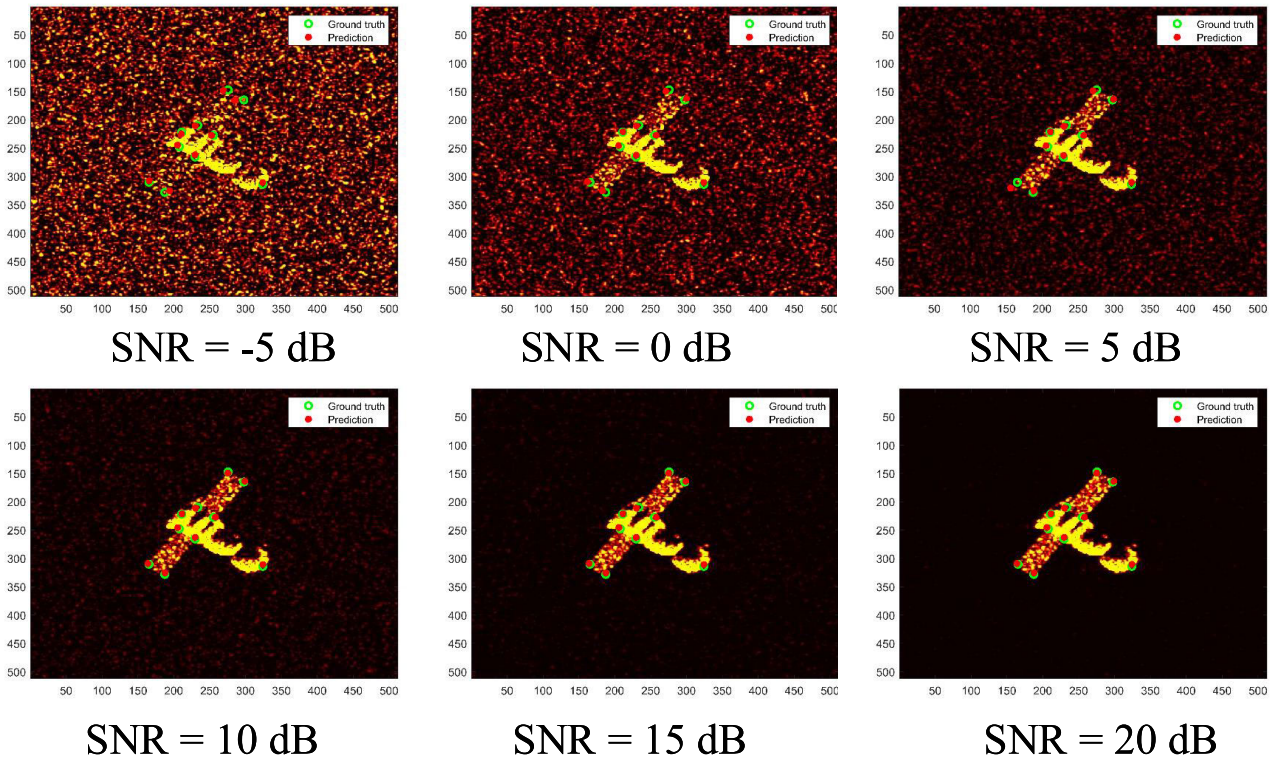

Fig. 9. Extraction results of Soyuz in different noise conditions.

TABLE IV
THE ESTIMATION RESULTS OF SPINNING TG-I

Observation Time	Estimation Error of the Body(degrees)	Estimation Error of the Solar Wing(degrees)	Estimation Error of Spin Shaft (degrees)	Estimation Error of Spin Speed(rad/s)
The proposed method				
Time 1	0.820	1.234	9.784	0.008
Time 2	1.304	2.335	13.795	0.010
Time 3	0.905	1.402	4.183	0.006
Time 4	1.467	1.012	12.254	0.009
Time 5	0.928	3.122	5.658	0.011
Time 6	1.878	2.413	15.091	0.012
Time 7	0.430	0.845	7.689	0.010
Time 8	0.550	0.384	12.932	0.007
Time 9	1.823	0.819	13.444	0.006
The ground-based method				
Time 1	3.232	2.985	8.648	0.007
Time 2	1.598	3.165	9.325	0.005
Time 3	2.005	4.315	11.954	0.010
Time 4	2.365	2.954	6.287	0.003
Time 5	0.879	1.315	4.042	0.009
Time 6	1.324	3.165	9.307	0.008
Time 7	1.112	2.227	7.239	0.001
Time 8	2.721	4.626	10.342	0.005
Time 9	3.419	2.097	13.625	0.011

- Second, target dynamic parameters are estimated by the proposed algorithm in a typical bi-station spaceborne ISAR observation.
- In the end, we demonstrate the advantages of the proposed method by comparing it with the existing ground-based method.

A. The Automatic Feature Extraction in ISAR Images

First of all, a simulation dataset is generated to investigate the feasibility of the proposed algorithm. The 3D surface of the observed satellite, TG-I, is divided into thousands of equivalent triangular facets, and the fast physical optics (FPO) algorithm is adopted to calculate the satellites echo at a given imaging angle [44], [45]. Then, the RD imaging algorithm is used to generate the ISAR image of the satellite. The main parameters of the radar system are given in Table I. In order to improve the visual similarity of the simulation image to the measured one, the signal-to-noise ratio (SNR) of each ISAR image is set to be 10 dB. In this way, more than 1200 ISAR images are simulated from different observation angles. After eliminating the ISAR images in which the image feature of key points is not complete, we use the rest of images as the training dataset, which consists of 800 images.

The trained key point extraction network is used to extract the vertices of solar wings and the endpoints of the target symmetry axis in the images. Then, the projection lengths of TG-I can be determined according to these key points after shape fitting. Nine images are simulated as the test samples to investigate the extraction performance of the network. The extraction result is given in Fig. 7, and the numerical comparison between the automatic extraction result and the ground truth is listed in Table II. From the comparison results, the mean bias is under 5 pixels, which demonstrates the high credibility and accuracy of the adopted network in projection feature extraction.

In order to investigate the robustness of a well-trained network, target key points are extracted from the same pose ISAR image under different SNR conditions. As shown in Fig. 8, the key point extraction results are still close to the true value when SNR decreases to -5 dB. Thus, the robustness of the proposed key point extraction method is confirmed.

Besides, another space target, Soyuz, is used to illustrate the generality of the proposed method for different targets. Additional 200 images of Soyuz are simulated as training samples to fine-tune the extraction network trained by TG-I samples. The extraction results in the Fig. 9 show that the proposed method is also feasible for other similar targets when the network is retrained by the additional samples.

B. The Instantaneous Dynamic Estimation of TG-I

To exemplify the proposed target dynamic estimation algorithm, a bi-station spaceborne ISAR observation scene is built in the STK software, as shown in Fig. 10. TG-I is chosen as the target satellite, and its orbit parameters are the same as one of the public OPS-SAT satellites at the height of 1400 km. After the target instantaneous position in the ECEF coordinate system is determined, two adjacent satellites on a 550-km orbit of the Starlink constellation are selected as the synchronous imaging observers. The TLE parameters of these three satellites are listed in Table. III. The radar LOS parameters of this observation system are shown in Fig. 11(a). The synchronous imaging moments when the two ISAR images have similar resolutions are depicted in red.

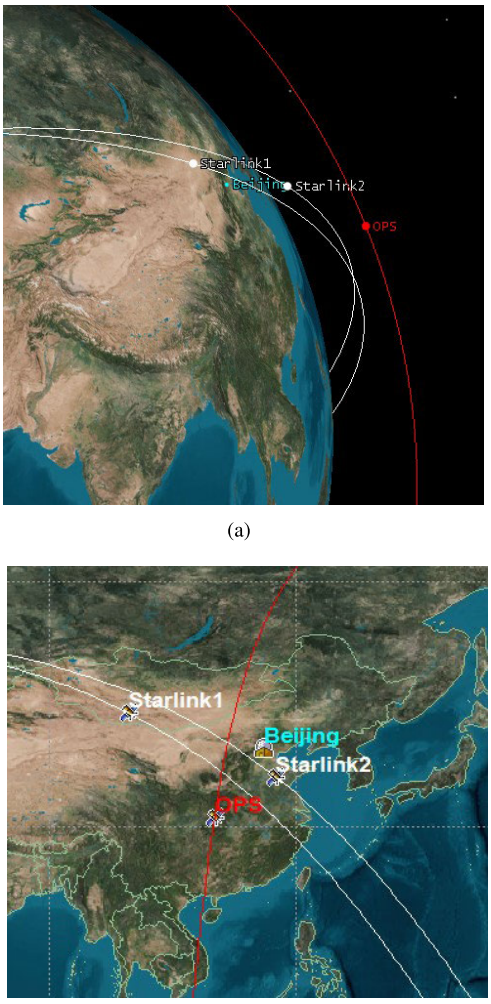

Fig. 10. The observation geometry of the spin satellite. (a) The bi-station spaceborne ISAR observation in the 3D world. (b) The sub-satellite point trajectorys of observers and target satellite.

The target satellite is set to spin around a certain shaft at a constant speed during each imaging period. The projection lengths of the target body and solar wing are extracted by the proposed automatic method and substituted into the instantaneous attitude optimization Eq. (8). Then, the estimated result of target instantaneous attitude are substituted into Eq. (13) to solve the target spin parameters including the rotation shaft and rotation speed. The estimation result is given in Table IV. As the numerical estimation results are close to the true values at these nine moments, the veracity of the attitude estimation is confirmed. Although the performance of spin parameter estimation can't compete with that of the three-station method, the estimation result is still can be accepted in practical applications.

C. Comparison Experiment

In this part, the advantage of the proposed algorithm is investigated by the comparison experiment with the existing work on the ground-based ISAR observation [20]. In [20], the projection lengths of target structures in multiple-station

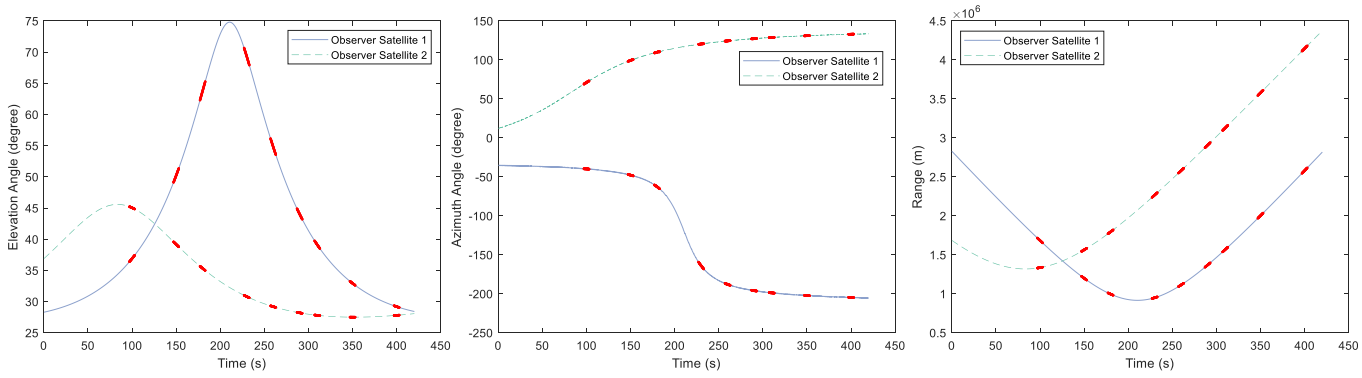

(a)

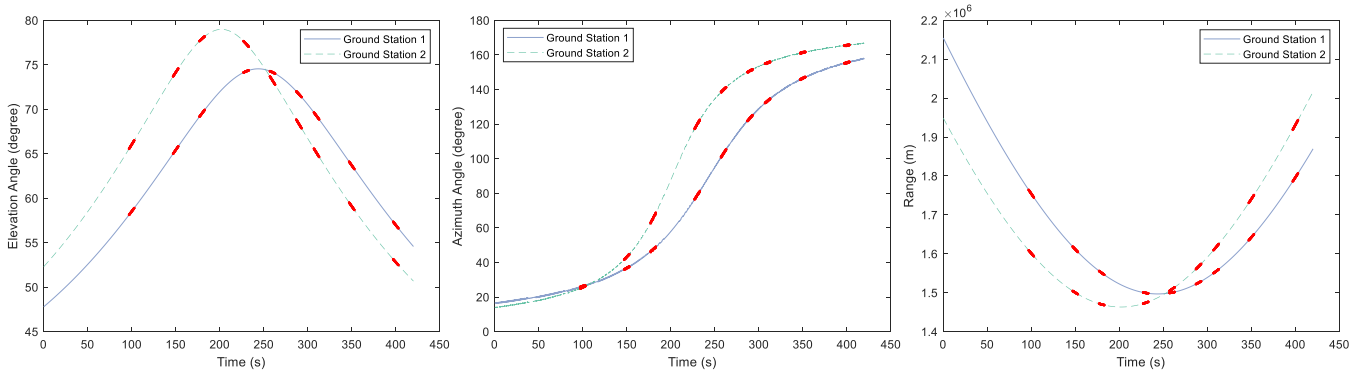

(b)

Fig. 11. Radar LOS parameters of the bi-station observation. (a) By the bi-station spaceborne ISAR observation. (b) By the bi-station ground-based ISAR observation.

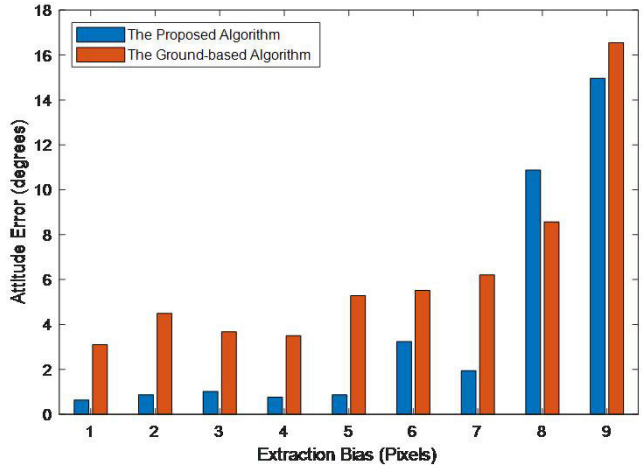

Fig. 12. Attitude estimation error comparison between the proposed algorithm and the existing ground-based algorithm.

TABLE V
THE SIGHT DIFFERENCE COMPARISON OF SYNCHRONOUS IMAGING BETWEEN TWO METHODS

Moments	The spaceborne system	The ground-based system
Time 1	111.0198	6.7871
Time 2	33.0153	9.2422
Time 3	13.4644	18.6105
Time 4	81.7333	138.9185
Time 5	51.8079	36.8102
Time 6	38.8598	27.4392
Time 7	33.6373	22.2692
Time 8	27.0633	15.4408
Time 9	22.3694	10.8092

ISAR images are utilized to estimate target attitude and spin parameters.

The main advantage of the proposed spaceborne method is extending the observation area for a certain target. From the published work [36], the available observation period for a ground-based radar system normally is dozens of minutes. In order to obtain high-resolution RD images, the coherent processing interval of a single image is about dozens of seconds for an LEO target. However, in the task of monitoring an HEO satellite, the coherent processing interval rapidly increases because the relative motion between the ground radar and the target decreases. By contrast, an alternative approach is presented using spaceborne radars. With the development of meta constellations, adjacent-orbit satellites can provide long-term ISAR imaging for a certain satellite.

Besides, for the LEO observation, the angular diversity of the spaceborne system performs better. Take the previous observation scene of the 1400 km-height

Algorithm 1 CGOA algorithm for parameter estimation

Input :

The search boundary of the optimization: ϖ
The maximum iteration: ε_1
Minimum move distance: ε_2
Control parameters: P and b
Attractive parameters: f and l

/* Parameters Initialization */

Randomly generate a particle swarm Λ according to ϖ

Initial cost value: $Pbest = 10$

Iteration number: $k = 1$

/* CGOA Algorithm */

while $\left|\vec{X}_{best}(k) - \vec{X}_{best}(k-1)\right| \geq \varepsilon_1 \text{or} k = \varepsilon_2$ **do**

/* Find best particle in the Swarm */

for $\vec{X}_i(k) \in \Lambda$ **do**

if $J\left(\vec{X}_i(k)\right) \leq Pbest$ **then**

$Pbest = J\left(\vec{X}_i(k)\right)$

$\vec{X}_{best}(k) = \vec{X}_i(k)$

end

end

/* Swarm Update */

for $\vec{X}_i(k) \in \Lambda$ **do**

/* Gap Update */

$\vec{\mathbf{h}}_{i,j}(k) = \vec{X}_j(k) - \vec{X}_i(k)$

$s\left(\left|\vec{\mathbf{h}}_{i,j}(k)\right|\right) = fe^{\frac{\left|\vec{\mathbf{h}}_{i,j}(k)\right|}{l}} - e^{-\left|\vec{\mathbf{h}}_{i,j}(k)\right|}$

/* Chaotic Map */

$c_1(k+1) = \left(c_1(k) + b - \frac{P}{2\pi}\sin(2\pi c_1(k))\right) \bmod (1)$

$c_2(k+1) = \left(c_2(k) + b - \frac{P}{2\pi}\sin(2\pi c_2(k))\right) \bmod (1)$

/* Particle Position Update */

$$\vec{X}_i(k+1) = c_1(t)\left(\sum_{j=1.j\neq i}^{N} c_2(t)s\left(\left|\vec{\mathbf{h}}_{i,j}(k)\right|\right)\frac{\vec{\mathbf{h}}_{i,j}(k)}{\left|\vec{\mathbf{h}}_{i,j}(k)\right|}\right) + \vec{X}_{best}(k)$$

end

$k = k + 1$

end

Output:

The ideal particle: $\vec{X}$

satellite for an example. Two ground-based stations are placed in Beijing (39.9 N,116.4 E,88 m) and Shijiazhuang (38.0 N,114.5 E,0 m), respectively. The radar LOS parameters of these two ground-based ISAR observation are calculated, as shown in Fig. 11(b). These two ground ISAR devices replace the spaceborne system to estimate target dynamic parameters in the similar way. And the numerical comparison is also given in Table IV. We also calculate the synchronous imaging angular difference results of the proposed method and the ground-based method, and the result is listed in Table V. The angular difference of the spaceborne system is bigger than that of the ground-based system at most moments except the pass-over period. It indicates that more observation information can be obtained from the spaceborne observation.

On the other hand, the proposed algorithm also performs better in solving target dynamic parameter optimization. As the feature extraction of target projection lengths is an intermediate product for both the proposed algorithm and the existing algorithm [20], same-level extraction accuracy should be ensured when the attitude estimation performances of these two methods are compared. In the same condition of feature extraction accuracy, each algorithm is implemented ten times for nine different attitude parameters. The attitude estimation

errors of the body and solar wing are averaged to evaluate the accuracy of the target dynamic estimation, as shown in Fig. 12. It is confirmed that the proposed spaceborne algorithm performs better. Because the spaceborne system provides a larger imaging sight difference. In order to reflect the robustness of the whole-lap observation period, we compare the manifolds of the observation matrix in these two observation scenes. The observation matrix $\mathbf{A}$ is defined as follows.

$$\mathbf{A} = \left[\vec{\mathbf{k}}_1 \ \cdots \ \vec{\mathbf{k}}_9 \right]^{\mathrm{T}} \tag{24}$$

$$\kappa(\mathbf{A}) = \frac{\max \frac{\|\mathbf{A}x\|}{\|x\|}}{\min \frac{\|\mathbf{A}x\|}{\|x\|}} \tag{25}$$

where $\kappa(\mathbf{A})$ refers to the matrix condition number.

Based on the SVD algorithm, the observation manifold of the spaceborne system is 6.1376, while that of the ground-based system is 8.8132. As a result, the proposed algorithm is more robust when the extraction bias of the target projection feature exists. As the target spin estimation is based on the target attitude estimation result, the reliability of the proposed algorithm also has a better performance in this stage.

V. Conclusion

In this paper, in order to achieve the dynamic estimation of on-orbit satellites, an approach was proposed based on synchronous spaceborne ISAR images. With the geometric projection of bi-station observations, an explicit expression was derived to connect the dynamic target parameters and its external observed RD images. Based on the target projection features extracted by the key points network, target dynamic parameters were determined in two optimizations using CGOA. The simulation results have illustrated the feasibility of the proposed algorithm in a typical LEO observation scene. Compared with the existing ground-based methods, the observation angular diversity of the proposed algorithm is analyzed. It can be considered as the biggest advantage of the proposed automatic dynamic estimation framework. We believe this work provides an effective approach to monitoring target dynamics on-orbit under the background of constellation situational security. However, at the current stage, the proposed feature extraction network hardly can be extended for other satellites with different structural features. That is to say the feature extraction network needs to be re-trained from scratch for the different targets. Besides, it also needs to be further investigated to achieve real-time monitoring of HEO satellites.

Appendices

The details of **Algorithm 1** is shown.

Acknowledgment

The authors would like to thank the anonymous reviewers for their valuable comments to improve the article quality.

References

[1] N. Bobrinsky and L. D. Monte, "The space situational awareness program of the European Space Agency," *Cosmic Res.*, vol. 48, no. 5, pp. 392–398, 2010.

[2] R. Xu et al., "Exploration of blockchain-enabled decentralized capability-based access control strategy for space situation awareness," *Proc. SPIE*, vol. 58, no. 4, 2019, Art. no. 041609.

[3] J. Radtke, C. Kebschull, and E. Stoll, "Interactions of the space debris environment with mega constellations—Using the example of the OneWeb constellation," *Acta Astronaut.*, vol. 131, pp. 55–68, 2017.

[4] S. Le May, S. Gehly, B. A. Carter, and S. Flegel, "Space debris collision probability analysis for proposed global broadband constellations," *Acta Astronaut.*, vol. 151, pp. 445–455, Oct. 2018.

[5] A. Boley and M. Byers, "Satellite mega-constellations create risks in low Earth orbit, the atmosphere and on Earth," *Sci. Rep.*, vol. 11, no. 1, pp. 1–8, 2021.

[6] V. Pesce, M. F. Haydar, M. Lavagna, and M. Lovera, "Comparison of filtering techniques for relative attitude estimation of uncooperative space objects," *Aerosp. Sci. Technol.*, vol. 84, pp. 318–328, Jan. 2019.

[7] T. Kouyama, A. Kanemura, S. Kato, N. Imamoglu, T. Fukuhara, and R. Nakamura, "Satellite attitude determination and map projection based on robust image matching," *Remote Sens.*, vol. 9, no. 1, 2017, Art. no. 90.

[8] D. Kucharski et al., "Attitude and spin period of space debris Envisat measured by satellite laser ranging," *IEEE Trans. Geosci. Remote Sens.*, vol. 52, no. 12, pp. 7651–7657, Dec. 2014.

[9] J. Pittet, J. Silha, and T. Schildknecht, "Spin motion determination of the Envisat satellite through laser ranging measurements from a single pass measured by a single station," *Adv. Space Res.*, vol. 64, no. 4, pp. 1121–1131, 2018.

[10] G. Kirchner, W. Hausleitner, and E. Cristea, "Ajisai spin parameter determination using Graz kilohertz satellite laser ranging data," *IEEE Trans. Geosci. Remote Sens.*, vol. 45, no. 1, pp. 201–205, Jan. 2007.

[11] N. Koshkin, E. Korobeynikova, L. Shakun, S. Strakhova, and Z. H. Tang, "Remote sensing of the EnviSat and Cbers-2B satellites rotation around the centre of mass by photometry," *Adv. Space Res.*, vol. 58, no. 3, pp. 358–371, 2016.

[12] R. Perrier, E. Arnaud, P. Sturm, and M. Ortner, "Estimation of an observation satellite's attitude using multimodal pushbroom cameras," *IEEE Trans. Pattern Anal. Mach. Intell.*, vol. 37, no. 5, pp. 987–1000, May 2015.

[13] S. Lemmens, H. Krag, J. Rosebrock, and I. Carnelli, "Radar mappings for attitude analysis of objects in orbit," in *Proc. 6th Eur. Conf. Space Debris*, Darmstadt, Germany, 2013, pp. 20–24.

[14] S. Lemmens and H. Krag, "Sensitivity of automated attitude determination form ISAR radar mappings," in *Proc. Adv. Maui Opt. Space Surveill. Technol. (AMOS) Conf.*, 2013, pp. 1–12.

[15] J. Rosebrock, "Absolute attitude from monostatic radar measurements of rotating objects," *IEEE Trans. Geosci. Remote Sens.*, vol. 49, no. 10, pp. 3737–3744, Oct. 2011.

[16] W. J. Zhong, J. S. Wang, W. J. Ji, X. Lei, and X. W. Zhou, "The attitude estimation of three-axis stabilized satellites using hybrid particle swarm optimization combined with radar cross section precise prediction," *Proc. Inst. Mech. Eng. G, J. Aerosp. Eng.*, vol. 31, no. 2, pp. 222–224, 2015.

[17] M. Ferrara, G. Arnold, and M. Stuff, "Shape and motion reconstruction from 3D-to-1D orthographically projected data via object-image relations," *IEEE Trans. Pattern Anal. Mach. Intell.*, vol. 31, no. 10, pp. 1906–1912, Oct. 2009.

[18] E. Mcfadden, B. Zhang, and M. Xing, "Three-dimensional reconstruction from ISAR sequences," *Proc. SPIE*, vol. 4744, no. 1, pp. 58–68, Jul. 2002.

[19] F. Wang, F. Xu, and Y.-Q. Jin, "Three-dimensional reconstruction from a multiview sequence of sparse ISAR imaging of a space target," *IEEE Trans. Geosci. Remote Sens.*, vol. 56, no. 2, pp. 611–620, Feb. 2018.

[20] Y. Zhou, L. Zhang, and Y. Cao, "Dynamic estimation of spin spacecraft based on multiple-station ISAR images," *IEEE Trans. Geosci. Remote Sens.*, vol. 58, no. 4, pp. 2977–2989, Apr. 2020.

[21] Y. Zhou, L. Zhang, S. Wei, and Y. Cao, "Dynamic analysis of spin satellites through the quadratic phase estimation in multiple-station radar images," *IEEE Trans. Comput. Imag.*, vol. 6, pp. 894–907, 2020.

[22] K. Suwa, T. Wakayama, and M. Iwamoto, "Three-dimensional target geometry and target motion estimation method using multistatic ISAR movies and its performance," *IEEE Trans. Geosci. Remote Sens.*, vol. 49, no. 6, pp. 2361–2373, Jun. 2011.

[23] P. Kou, Y. Liu, W. Zhong, B. Tian, W. Wu, and C. Zhang, "Axial attitude estimation of spacecraft in orbit based on ISAR image sequence," *IEEE J. Sel. Topics Appl. Earth Observ. Remote Sens.*, vol. 14, pp. 7246–7258, 2021.
[24] Y. Zhou, S. Wei, L. Zhang, W. Zhang, and Y. Ma, "Dynamic estimation of spin satellite from the single-station ISAR image sequence with the hidden Markov model," *IEEE Trans. Aerosp. Electron. Syst.*, vol. 58, no. 5, pp. 4626–4638, Oct. 2022.
[25] Y. Huang et al., "HRWS SAR narrowband interference mitigation using low-rank recovery and image-domain sparse regularization," *IEEE Trans. Geosci. Remote Sens.*, vol. 60, 2022, Art. no. 5217914.
[26] Y. Zhou, L. Zhang, Y. Cao, and Z. Wu, "Attitude estimation and geometry reconstruction of satellite targets based on ISAR image sequence interpretation," *IEEE Trans. Aerosp. Electron. Syst.*, vol. 55, no. 4, pp. 1698–1711, Aug. 2019.
[27] Y. Du and Y. Jiang, "Parametric translational motion compensation of spaceborne ISAR imagery for Earth-orbit targets based on parabola detection and entropy minimization," *Remote Sens. Lett.*, vol. 12, no. 2, pp. 160–168, 2021.
[28] E. Marchetti, A. Stove, E. Hoare, M. Cherniakov, and M. Gashinova, "Images of satellite elements with a space-borne sub-THz ISAR system," in *Proc. 18th Eur. Radar Conf. (EuRAD)*, 2022, pp. 425–428.
[29] R. Cao, Y. Wang, and Y. Zhang, "Analysis of the imaging projection plane for ship target with spaceborne radar," *IEEE Trans. Geosci. Remote Sens.*, vol. 60, 2022, Art. no. 5205021.
[30] X. Yang, Y. Pi, T. Liu, and H. Wang, "Three-dimensional imaging of space debris with space-based terahertz radar," *IEEE Sensors J.*, vol. 18, no. 3, pp. 1063–1072, Feb. 2018.
[31] Z. Wu, C. Shen, and A. Van Den Hengel, "Wider or deeper: Revisiting the ResNet model for visual recognition," *Pattern Recognit.*, vol. 90, pp. 119–133, Jun. 2019.
[32] C. Szegedy, S. Ioffe, V. Vanhoucke, and A. Alemi, "Inception-v4, inception-ResNet and the impact of residual connections on learning," in *Proc. 31st AAAI Conf. Artif. Intell.*, 2017, pp. 1–7.
[33] P. Xie, L. Zhang, C. Du, X. Wang, and W. Zhong, "Space target attitude estimation from ISAR image sequences with key point extraction network," *IEEE Signal Process. Lett.*, vol. 28, pp. 1041–1045, 2021.
[34] S. Saremi, S. Mirjalili, and A. Lewis, "Grasshopper optimisation algorithm: Theory and application," *Adv. Eng. Softw.*, vol. 105, pp. 30–47, Mar. 2017.
[35] S. Arora and P. Anand, "Chaotic grasshopper optimization algorithm for global optimization," *Neural Comput. Appl.*, vol. 31, no. 8, pp. 4385–4405, Aug. 2019.
[36] FGAN Lab. (Mar. 2018). *Forscher des Fraunhofer FHR Begleiten Wiedereintritt der Chinesischen Raumstation Tiangong-1*. [Online]. Available: https://www.fhr.fraunhofer.de/tiangong-bilder
[37] J. T. Mayhan, M. L. Burrows, K. M. Cuomo, and J. E. Piou, "High resolution 3D 'snapshot' ISAR imaging and feature extraction," *IEEE Trans. Aerosp. Electron. Syst.*, vol. 37, no. 2, pp. 630–642, Apr. 2001.
[38] Y. Lee and J. P. Choi, "Connectivity analysis of mega-constellation satellite networks with optical intersatellite links," *IEEE Trans. Aerosp. Electron. Syst.*, vol. 57, no. 6, pp. 4213–4226, Dec. 2021.
[39] A. Nardin, J. Fraire, and F. Dovis, "Contact plan design for GNSS constellations: A case study with optical inter-satellite links," *IEEE Trans. Aerosp. Electron. Syst.*, vol. 58, no. 3, pp. 1981–1995, Jun. 2021.
[40] E. Insafutdinov, L. Pishchulin, B. Andres, M. Andriluka, and B. Schiele, "DeeperCut: A deeper, stronger, and faster multi-person pose estimation model," 2016, *arXiv:1605.03170*.
[41] E. Insafutdinov et al., "ArtTrack: Articulated multi-person tracking in the wild," in *Proc. IEEE Conf. Comput. Vis. Pattern Recognit.*, Honolulu, HI, USA, Jul. 2017, pp. 1293–1301.
[42] Y. Chen, C. Shen, X. Wei, L. Liu, and J. Yang, "Adversarial PoseNet: A structure-aware convolutional network for human pose estimation," in *Proc. IEEE Int. Conf. Comput. Vis.*, Venice, Italy, Oct. 2017, pp. 1221–1230.
[43] P. Xie, L. Zhang, Y. Ma, Y. Zhou, and X. Wang, "Attitude estimation and geometry inversion of satellite based on oriented object detection," *IEEE Geosci. Remote Sens. Lett.*, vol. 19, pp. 1–5, 2022.
[44] F. Wang, T. F. Eibert, and Y. Q. Jin, "Simulation of ISAR imaging for a space target and reconstruction under sparse sampling via compressed sensing," *IEEE Trans. Geosci. Remote Sens.*, vol. 53, no. 6, pp. 3432–3441, Jun. 2015.
[45] A. F. Garcia-Fernandez, O. A. Yeste-Ojeda, and J. Grajal, "Facet model of moving targets for ISAR imaging and radar back-scattering simulation," *IEEE Trans. Aerosp. Electron. Syst.*, vol. 46, no. 3, pp. 1455–1467, Jul. 2010.

Yejian Zhou was born in Zhejiang, China, in 1993. He received the B.S. degree in electronic engineering and the Ph.D. degree in signal processing from Xidian University, Xi'an, China, in 2015 and 2020, respectively. He was a Visiting Ph.D. Student with the Department of Urban Planning and Environment, KTH Royal Institute of Technology, from September 2019 to August 2020. He is currently an Assistant Professor with the College of Information Engineering, Zhejiang University of Technology. His research interests include ISAR imaging and image interpretation.

Pengfei Xie was born in Henan, China, in 1992. He received the M.S. degree in electronics and communication engineering from Xidian University in 2019. He is currently pursuing the Ph.D. degree in signal and information processing with the School of Electronics and Communication Engineering, Sun Yat-sen University. His research interests include radar imaging and target detection.

Chenwei Li was born in Inner Mongolia Autonomous Region, China, in 1998. He received the B.S. degree in electronic engineering and automation from Northeast Petroleum University in 2020. He is currently pursuing the M.S. degree with the School of Information Engineering, Zhejiang University of Technology. His research interests include image fusion and target recognition.

Mao Jian was born in Inner Mongolia Autonomous Region, China, in 1991. He received the B.S. degree in information science and electronic engineering from Zhejiang University, China, in 2014, and the M.S. degree from the Graduate School, Second Academy of China Aerospace, in 2017. He is currently an Assistant Researcher with the Laboratory of Pinghu, Beijing Institute of Infinite Electric Measurement. His research interests include radar imaging and signal processing.

Lei Zhang was born in Zhejiang, China, in 1984. He received the Ph.D. degree in signal processing from Xidian University in 2012. He is currently working as a Professor with the School of Electronics and Communication Engineering, Sun Yat-sen University (Shenzhen Campus). His research interests include radar imaging (SAR/ISAR) and motion compensation.

Wenan Zhang (Member, IEEE) was born in Zhejiang, China, in 1982. He received the B.S. degree in automation and the Ph.D. degree in control theory and control engineering from the Zhejiang University of Technology, Hangzhou, in 2004 and 2010, respectively. From 2010 to 2011, he was a Senior Research Associate with the Department of Manufacturing Engineering and Engineering Management, City University of Hong Kong, Hong Kong. Since 2020, he has been with the Zhejiang University of Technology, where he is currently a Professor with the Department of Automation. His current research interests include multi-sensor information fusion estimation and robotics. He was awarded an Alexander von Humboldt Fellowship in 2011. Since September 2016, he has been a Subject Editor of *Optimal Control Applications and Methods*.